Energies **2014**, *7*, 8483-8507; doi:10.3390/en7128483

OPEN ACCESS

energies

ISSN 1996-1073

www.mdpi.com/journal/energies

Article

On-Site Radon Detection of Mining-induced Fractures from Overlying Strata to the Surface: A Case Study of the Baoshan Coal Mine in China

Wei Zhang [1,2,3,*], Dong-Sheng Zhang [4], Li-Xin Wu [1,2,3] and Hong-Zhi Wang [4]

[1] IoT Perception Mine Research Center, China University of Mining & Technology, Xuzhou 221008, China; E-Mail: awulixin@263.net

[2] The National and Local Joint Engineering Laboratory of Internet Application Technology on Mine, Xuzhou 221008, China

[3] School of Environment Science and Spatial Informatics, China University of Mining & Technology, Xuzhou 221116, China

[4] School of Mines, China University of Mining & Technology, Xuzhou 221116, China; E-Mails: dshzhang123@126.com (D.-S.Z.); cumterwhz@163.com (H.-Z.W.)

* Author to whom correspondence should be addressed; E-Mail: zhangwei@cumt.edu.cn; Tel.: +86-158-6218-7549; Fax: +86-516-8359-0501.

External Editor: Brian Agnew

Received: 26 September 2014; in revised form: 25 October 2014 / Accepted: 9 December 2014 / Published: 22 December 2014

Abstract: Large-scale longwall mining of shallow coal seams may cause mining-induced fractures that can project completely through to the surface. This could lead to a series of mine safety and environmental issues, further deteriorating the already fragile ecological environment in the Western mining areas in China. Therefore, an accurate and effective understanding of the spatiotemporal evolution law of mining-induced fractures in overlying strata and its relationship to upper aquifers is critical. In this paper, the application of the geophysical-chemical properties of radon in mining engineering is explored as a potential solution to the shortcomings of existing surveying methods. A radioactive measurement method is proposed for the detection of the development of mining-induced fractures from overlying strata to the surface in the Baoshan Coal Mine (BCM). The on-site test indicated that the first weighting step is approximately 60 m, the average periodic weighting step is approximately 20 m, and the influence coverage of the advanced abutment pressure is approximately 30 m. The presented method could be used

as an indirect technical support to increase the safety of coal mining by acting as a simple, fast, and reliable method of detecting mining-induced fractures in overlying strata.

Keywords: shallow coal seams; mine safety and environmental issues; radon detection; mining-induced fractures; on-site trial

1. Introduction

Coal, one of the main energy forms in China, accounts for approximately 77% and 65% of the county's energy production and consumption, respectively, thus playing an important role in China's economic development [1,2]. According to the latest coalfield prediction results provided by China's National Administration of Coal Geology (CNACG) [3], China's coal resources are mainly distributed throughout the West, e.g., Inner Mongolia, Xinjiang, Shaanxi, Shanxi, Ningxia, and Guizhou. Two major coal mining areas have been established in the Northwest and the Southwest, and are typically represented by Inner Mongolia and Guizhou [4,5]. Northwest China is an arid to semi-arid area, where the coal seams are typically shallow and covered by a thin layer of bedrock. In its natural state, the surface's ecological environment is fragile [6–8]. Large-scale longwall mining of shallow coal seams could cause mining-induced fractures to communicate with the surface immediately, leading to a series of mine safety and environmental issues, including crack formation, water loss, vegetation deterioration, land desertification, and spontaneous coal combustion, as shown in Figure 1. This can propel any potential ecological fragility into a state of actual destruction [9–11]. In Eastern China, many mines have begun exploiting the shallow coal found underneath Quaternary unconsolidated confined aquifers in order to relieve the tension of coal resources in the later mining stage [12–14]. Because the dynamic development of mining-induced fractures in overlying strata is difficult to understand, major water inrush accidents occur easily. Concurrently, due to overcrowding, buildings and farmlands have been damaged and the daily lives of the locals have been disrupted. Therefore, an accurate and effective understanding of the spatiotemporal evolution law of mining-induced fractures in overlying strata has become the theoretical basis of solving the above issues.

Currently, there are many numerical and physical simulation methods dedicated to the study of the development characteristics of mining-induced fractures in overlying strata [15–17]. However, in existing research, there are no reliable, effective, and operable detection methods for the dynamic development process of mining-induced fractures and the aquosity of overlying strata. The traditional three-zone theory [18] is no longer suitable for the shallow coal seams in Western China mining areas. Information as to whether the development of mining-induced fractures in overlying strata through the upper loose aquifer is critical to the success of aquifer protection mining in Western mining areas and unexploited coal mining in Eastern mining areas. Likewise, a valid surveying method is necessary to guarantee the effectiveness of corresponding mining control measures. Due to geological conditions, it is sometimes difficult to achieve the expected goals by using existing engineering methods, thus, the effective implementation of safe-efficient mining techniques suffers from significant interference. Therefore, the technological innovation of a method for the detection of mining-induced fractures development and the aquosity of overlying strata is urgently needed.

Figure 1. Mine safety and environmental issues due to underground coal mining: (**a**) formation of cracks on the surface; (**b**) water loss; (**c**) vegetation deterioration; (**d**) land desertification; (**e**) coal spontaneous combustion; (**f**) water inrush; (**g**) formation of cracks in architectural structures; and (**h**) farmland subsidence.

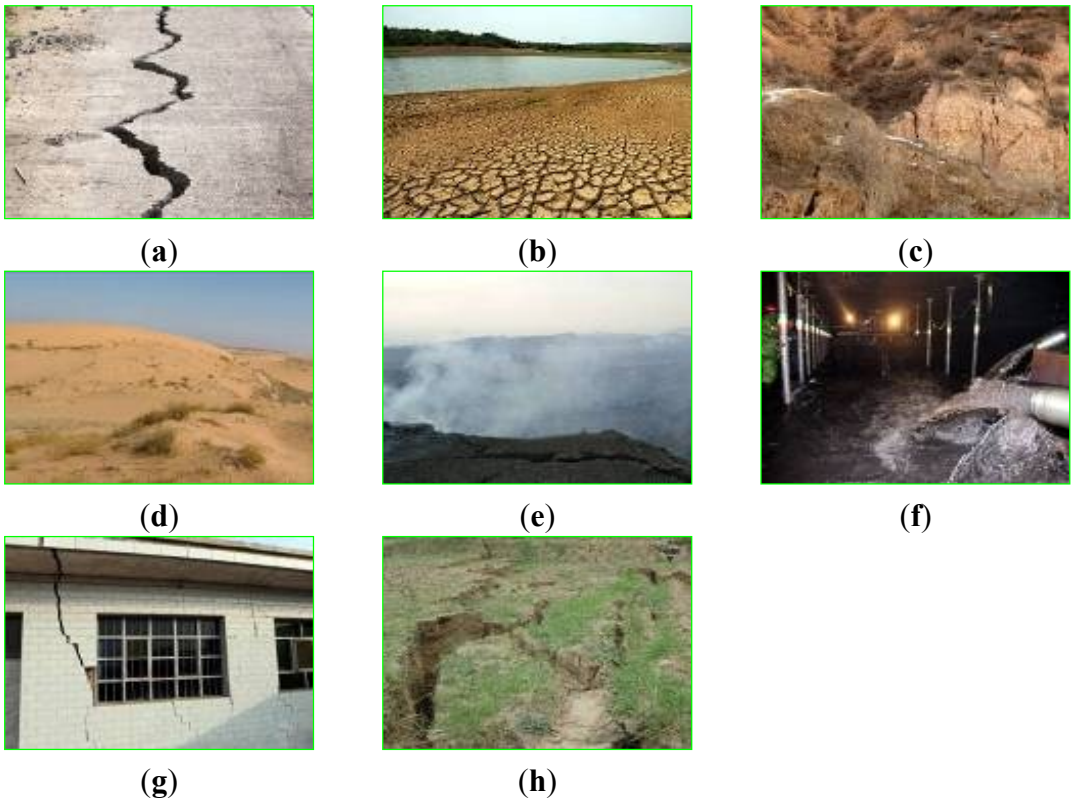

Radon is the only radioactive inert gas that is well-known to be in contact with humans. Because of its radioactivity, even if its concentration is low, radon levels are still measurable. In addition, due to the geochemical properties of inert gases, radon can accumulate and transport in micropores or microfractures [19,20]. Due to these two features (radioactivity and inertness), radon is detectable on the surface. For example, German scholars have found abnormal radon concentrations in the surface soil above mining-affected deep shaft mining areas [21]. Through predictions, the vertical migration distance has been estimated to be at least 400 m, though the detailed mining depth is not mentioned in this research. Like other nuclear-based techniques, the measurement of radon is based on the detection and measurement of the energy emitted in its radioactive decay, and combining this information with other relevant data, corresponding problems are analyzed. To seek a solution to these problems, our group has proposed a simple, fast and reliable method that applies the radon detection method in order to understand the development of mining-induced fractures and the aquosity of overlying strata [22–24]. In this paper, an on-site trial of radon detection of mining-induced fractures from overlying strata to the surface was performed in the 6203# coalface of the BCM in China, further verifying the feasibility of the radon detection method.

2. Mining and Geological Conditions

2.1. Location and Surface Morphology of the Study Area

The BCM is one of the mines in the Yitai Mining Area (YMA). The YMA exploits the shallow coal seams of the Shendong Coalfield (SC), which is located in the southwest of the Inner Mongolia Autonomous Region, northeast of Shaanxi Province. The SC, the largest proven coalfield in China, represents one of the world's eight largest coalfields. Proven coal reserves in this mining district equate to 223.6 billion tons, accounting for approximately a quarter of China's total coal reserves. In 2011, coal production from this mining district totaled more than 200 Mt. The shallow coal seams are comprised of Jurassic period coal within 100 m depths and are typically covered by a thin layer of bedrock with thick Aeolian sand.

The BCM is located between the 110°21'38" and 110°25'21" East longitudes and between the 39°25'49" and 39°29'55" North latitudes (shown in Figure 2). The surface elevation varies from 1315.8 m to 1142 m, with a maximum elevation difference of approximately 174 m. The highest elevation point (1315.8 m) lies near the northern boundary of the coal mine, and the lowest one (1142 m) lies near the Boniuchuan gully. The surface of the coal mine has no buildings, and is covered by a Quaternary unconsolidated formation, which mainly consists of barchan dunes (shown in Figure 3). Thus, the surface of this hilly area with undeveloped vegetation is typical to that of a plateau.

Figure 2. Location of the BCM in the YMA.

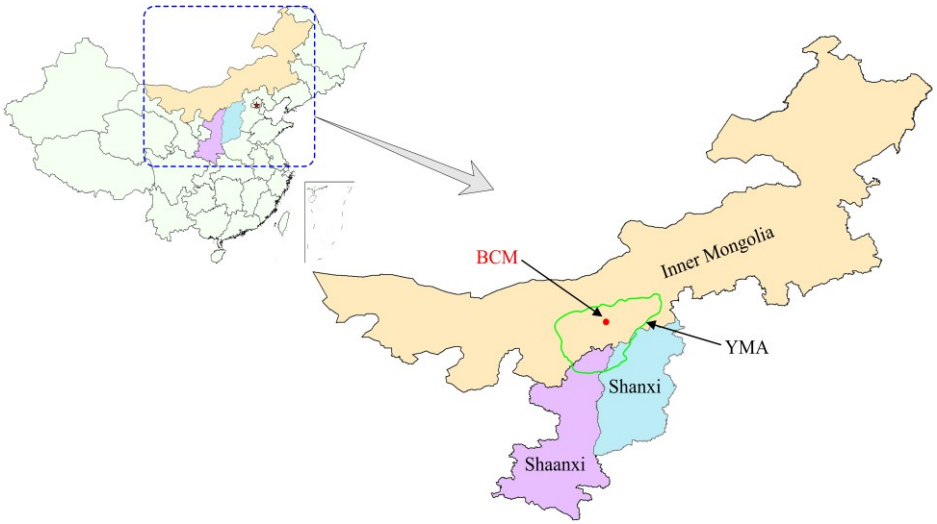

Figure 3. Surface morphology of the BCM: (**a**) overall perspective; (**b**) sandy vegetation; and (**c**) barchan dunes.

(**a**) (**b**) (**c**)

2.2. Mining and Geological Conditions of the 6203# Coalface

The 6203# coalface is located in the second panel of the BCM. The coalface, enveloped by two gateways (headgate and tailgate), is 2400 m long and 200 m wide with an area of 480,000 m^2, as shown in Figure 4. The elevation of the 6# coal seam floor varies from 1269 m to 1216 m, and the buried depth is about 90 m. The dip angle of the coal seam ranges from 1° to 4° with an average of 3°, the compressive strength from 4.0 MPa to 6.0 MPa with an average of 5.0 MPa, and the thickness from 4.3 m to 5.7 m with an average of 5.0 m. The single pass full height (5.0 m) longwall mining method is used to extract resources from the 6# coal seam. The immediate roof is comprised of broken silty mudstone, and the main roof is made up of hard packsand. As is typical of a key stratum, the main roof controls the movement of all its overlying strata. The immediate floor is also comprised of hard packsand. The placement and composition of the strata in the 6203# coalface are listed in Table 1.

Figure 4. Layout of the 6203# coalface.

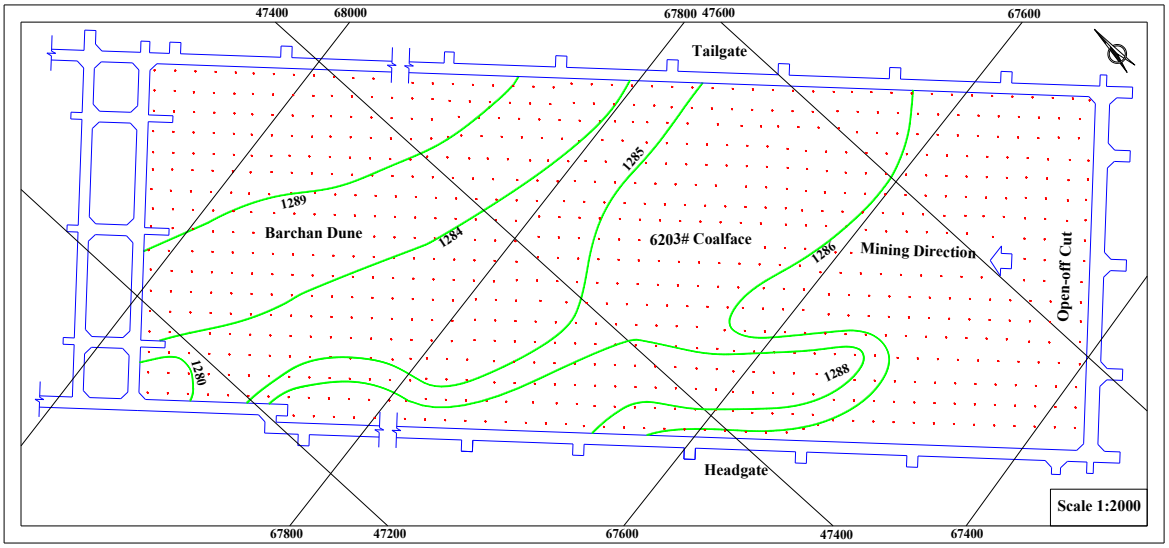

Table 1. The placement and composition of the strata in the 6203# coalface.

Sequence	Lithology	Thickness (m)	Depth (m)	Remarks
1	Aeolian sand	22.0	22.0	Aquifer located at the base
2	Mudstone	9.5	31.5	Aquiclude
3	Weathered sandstone	15.3	46.8	-
4	Sandy mudstone	9.2	56.0	-
5	Siltstone	7.7	63.7	-
6	Packsand	10.6	74.3	Main roof (Key stratum)
7	Silty mudstone	3.5	77.8	Immediate roof
8	Coal	5.0	82.8	6# coal seam
9	Packsand	6.8	89.6	Immediate floor

Coal ranks in the 6# coal seam are mostly comprised of non-caking coal, followed by long flame coal, two types which are optimally suited for use in the chemical industry and power plants. Beddings and joints are widespread in the coal seam, with two thin layers of gangue. The overall structural configuration of the coal seam in the coalface is monoclinal structure leans to southeast. This

configuration has led to a thickening trend in the coal seam from the north side to the south side. In the process of drivage construction of the headgate and tailgate, no large faults or other geological structures were found. The coalface has a wide, gentle curve shape and is part of a simple geological area. The hydrogeological condition of the coalface is also simple, and the normal amount of water inflow is 20 m^3 per hour.

3. Method of Radon Detection on the Surface

3.1. Steps for Radon Detection on the Surface

Comprehensively considering the fieldwork operability, as well as the structure and characteristics of the radon-measuring instruments, the entire process of radon detection on the surface can be divided into six steps, as shown in Figure 5.

Figure 5. Steps for radon detection on the surface.

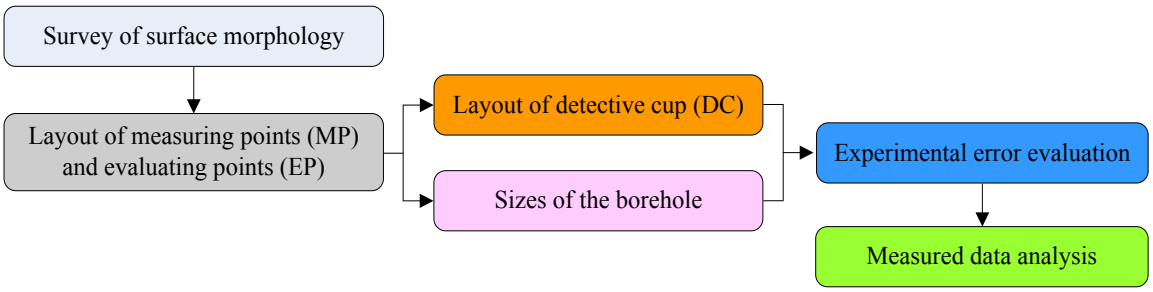

3.2. Layout Schemes of the Measuring Points (MP) and Evaluating Points (EP)

According to the surface topography of the 6203# coalface and the conditions of the adjacent 6202# and 6204# coalfaces, five measuring lines (ML) were laid along the strike direction of the coalface at 20 m intervals and were then labeled from right to left as lines 1 through 5. Next, 20 MP at 10 m intervals were labeled as 1 to 20 from the headgate to the tailgate. Then, the MP at lines 1 through 4 were measured with a CD-1/KZ-D02 *a* cup emanometer (CCE) (shown in Figure 6), and the MP at line 5 were measured with a KJD-2000R continuous emanometer (KCE) (shown in Figure 7). The CCE has greater sensitivity than 2 cpm/(Bq/m^3) with counter capacity 0 to 9999 while the KCE has greater sensitivity than is 1.3 cpm/(Bq/m^3) with measurement range 2 to 400,000 Bq/m^3. Prior to the use of the two devices ex works, both of them were calibrated in the standard radon chamber (SRC) of China's National Institute of Metrology (CNIM). The calibration process includes three steps: (1) a stable radon concentration will be produced in the SRC; (2) the benchmark instrument (AlphaGUARD PQ2000 emanometer) will be used; (3) a comparative measurement will be conducted, and the scale factor of the devices will be calibrated. To guarantee the measurement accuracy of the CCE and KCE, they will be sent periodically to the CNIM for inspection every six months. Due to the limits of detection time and construction conditions, detections of radon concentration at different depths in the strata are not performed. The layout parameters of the MP and EP are illustrated in Figure 8.

Figure 6. The photo of CCE.

Figure 7. The photo of KCE.

Figure 8. Layout schemes of the MP and EP.

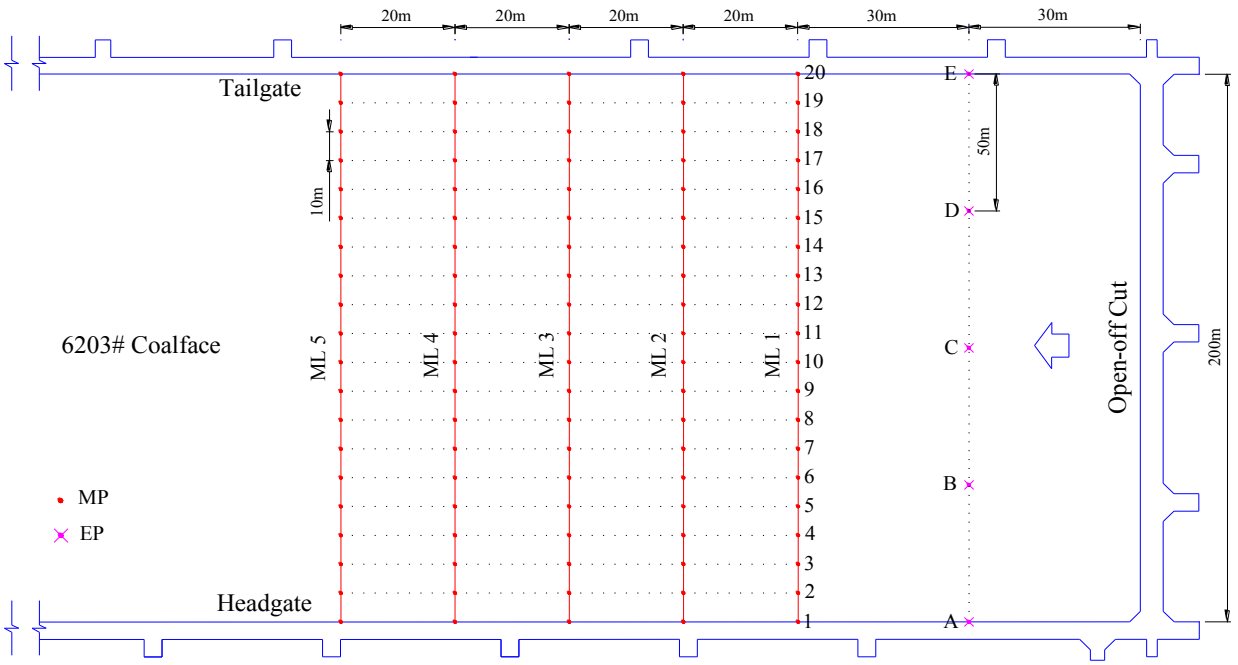

3.3. Layout of the Detective Cup (DC)

The DC of the CCE, which is used to collect the daughter products of radon decay, is made up of high adsorption materials with a collection area of 12 × 12 cm^2. A shallow pit, with depth of 30 cm to 40 cm and width of 20 cm, will be dug with a small shovel. Then, the DC will be placed inversely into the pit and covered with plastic film and buried with soil. The DC setup is shown in Figure 9. As a

general rule, the DC can be put into the CCE to measure after being buried for four hours. However, due to the limitations of field conditions, the DC is buried in the morning and measured after 24 h in the process of this test. The interval of the measurements could be 1 min, 2 min, or 3 min, but the counts of radon decay in 3 min are usually taken as the measured value of the MP. The benefit of this approach is that the measured values could be connected with the advance distance of coalface per day, which is convenient to the analysis of the measured data.

Figure 9. Layout of the DC.

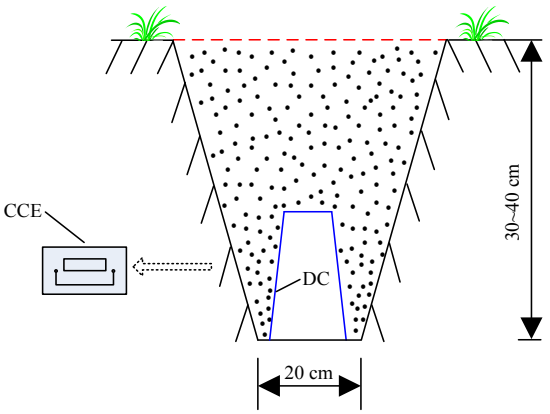

3.4. Sizes of the Borehole

The pumping pole (PP) of the KCE, which is used to pump the radon of the MP, has four small pumping holes (PH) on the pole head. A vertical borehole will be drilled by the drilling steel at a depth of 50 cm to 60 cm with a diameter of 3 cm, as shown in Figure 10.

When the borehole is finished, the PP will be rapidly inserted into the borehole, while four PH on the pole head will be kept unobstructed. Then, the soil is utilized to obstruct the interspace between the PP and the borehole wall in order to avoid a dilution effect caused by the surface air. Next, the rubber hose (RH) is used to connect the KCE to the PP. Lastly, the instrument is activated, and the on-site measurement is performed. Each MP will be continuously measured three times in five-minute increments. The third measurement will be regarded as the result of the MP.

Figure 10. Sizes of the borehole.

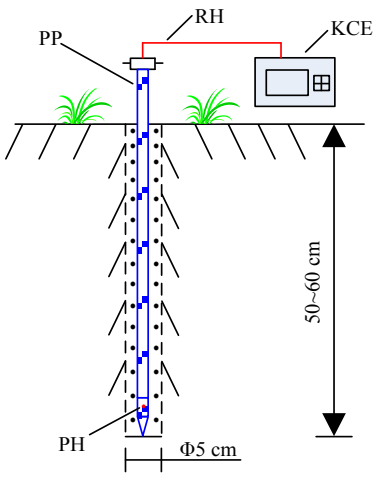

4. On-Site Radon Detection Trial and Measured Data Analysis

4.1. On-Site Radon Detection Trial

According to the measurement plans, all of the MP had to be placed on the surface of the 6203# coalface. The coalface has advanced from the open-off cut since 25 July 2011. Meanwhile, the CCE and KCE were used to detect the variation of radon concentration at the MP. Figure 11 depicts the technological process of the on-site radon detection trial.

Figure 11. The technological process of on-site radon detection trial: (**a**) dig the small pit; (**b**) lay the DC; (**c**) measure the counts; (**d**) adjust the device; (**e**) set the parameters; and (**f**) measure the concentrations.

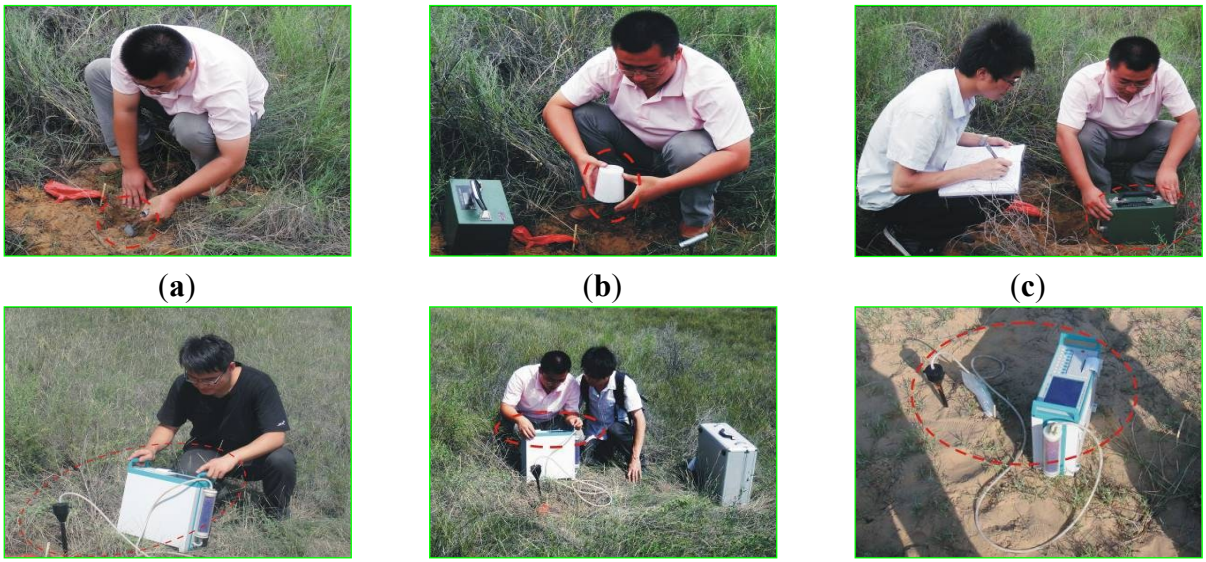

(**a**) (**b**) (**c**)

(**d**) (**e**) (**f**)

4.2. Measured Data Analysis

4.2.1. Experimental Error Evaluation

It is well-known that the radioactive measurement methods are simple, convenient and practicable. However, radioactive materials are composed of large radioactive atoms, whose radioactive decay has the features as contingency and randomness. Therefore, a statistical fluctuation phenomenon of radioactive decay frequently appears in the process of actual measurement, which causes a statistical fluctuation error and becomes the main source of experimental error [25]. In the case of no change in the characteristics of the strata, the radon measurement results will be greatly affected by environmental factors (which mainly include temperature, humidity and pressure). Under laboratory conditions, the above factors can be easily kept in a constant state. However, it is difficult to achieve the ideal state in the field survey. As a matter of fact, the daily variation of radon concentration can sometimes fluctuate up to 50% [26]. In order to evaluate the degree of influence on the subsequent measured data resulting from the natural fluctuation error, five EP with 30 m distances were laid beyond the 6203# coalface (shown in Figure 8). Before the 6203# coalface advanced, the radon concentration of evaluating points had been measured with the CCE for a

week. The variations of radon concentration of the EP have been shown in Figure 12. At the same time, the calculated results of the sample parameters (mainly includes the average value $\overline{x}$, standard deviation σ and coefficient of variation $\sigma / \overline{x}$) have been listed in Table 2. According to Figure 12 and Table 2, one can draw the conclusion that the degree of statistical fluctuation is small, and the coefficients of variation of the sample parameters are mostly within 2%. Therefore the experimental error will not significantly affect the subsequent measured data analysis.

Figure 12. The variations of radon concentration of the EP.

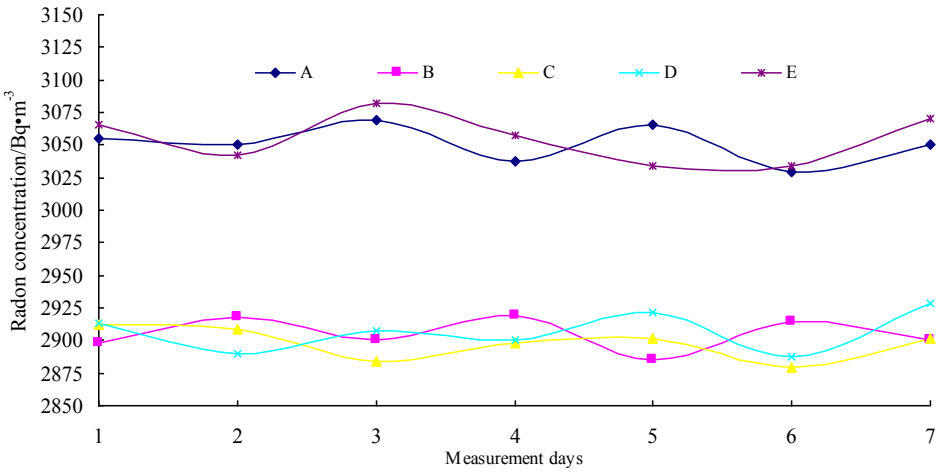

Table 2. The calculated results of the sample parameters.

EP	Average value $\overline{x}$	Standard deviation σ	Coefficient of variation $\sigma / \overline{x}$
A	3051	34.93	1.15%
B	2905	31.05	1.07%
C	2898	30.10	1.04%
D	2907	37.63	1.29%
E	3041	46.15	1.51%

4.2.2. Measured Data Analysis

In order to further eliminate causes of error in the measured data, such as instrument vibration interference and experimental error, the Daubechies wavelet was applied. This wavelet handles the measured data by a two-order discrete orthogonal wavelet transformation during the process of on-site detection. The combined advance distance of the 6203# coalface each day (listed in Table 3) and the variation features of the radon counts and concentrations within ML 1 through 5 from 25 July to 9 August are illustrated in Figures 13 and 14. Figure 13 is a three-dimensional stereogram of radon counts within ML 1 through 4, drawn by MATLAB mathematical software and interpolated by the cubic method according to the grid density. Figure 14 is a two-dimensional graph of the radon concentrations at ML 5, drawn by the Excel software based on the scatter values. Because the adjacent 6202# and 6204# coalfaces already had been mined, the lateral of abutment pressure was larger at the two ends of the 6203# coalface, as well as the overlying strata had caved in these areas, which would provide a large number of migration channels (mining-induced fractures) for radon near the headgate and tailgate. Therefore, this had caused the two ends to have values higher than the middle values.

Table 3. Advance distance of the 6203# coalface each day.

Date	Advance distance (m)	Date	Advance distance (m)
25 July	8.8	2 August	84.8
26 July	18.3	3 August	93.7
27 July	27.2	4 August	100.3
28 July	38.6	5 August	109.1
29 July	47.9	6 August	117.7
30 July	57.6	7 August	127.6
31 July	66.3	8 August	137.0
1 August	75.9	9 August	147.5

Figure 13. Variation features of the radon counts of ML 1 through 4: (**a**) 25 July; (**b**) 26 July; (**c**) 27 July; (**d**) 28 July; (**e**) 29 July; (**f**) 30 July; (**g**) 31 July; (**h**) 1 August; (**i**) 2 August; (**j**) 3 August; (**k**) 4 August; (**l**) 5 August; (**m**) 6 August; (**n**) 7 August; (**o**) 8 August; and (**p**) 9 August.

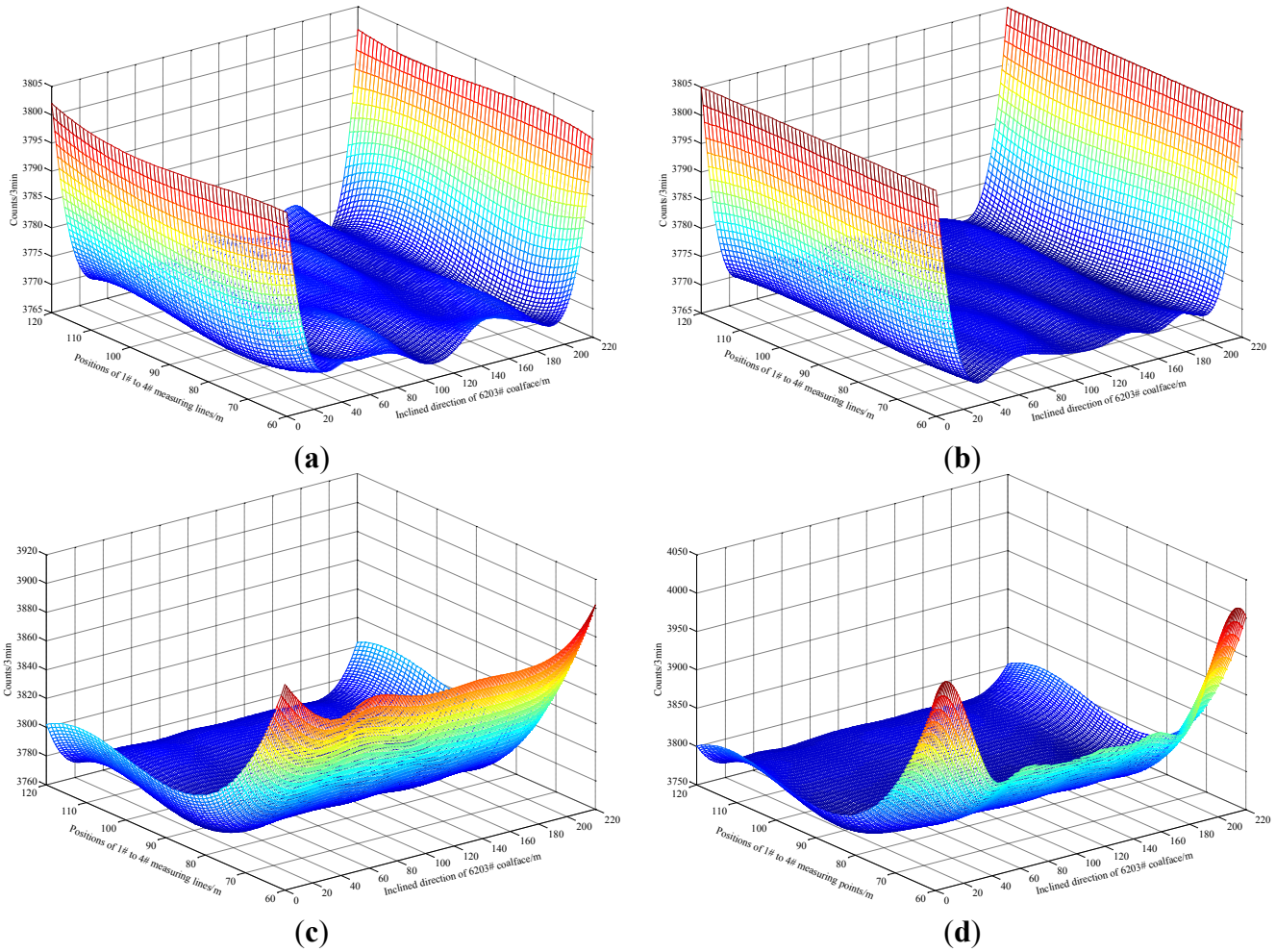

Figure 13. *Cont.*

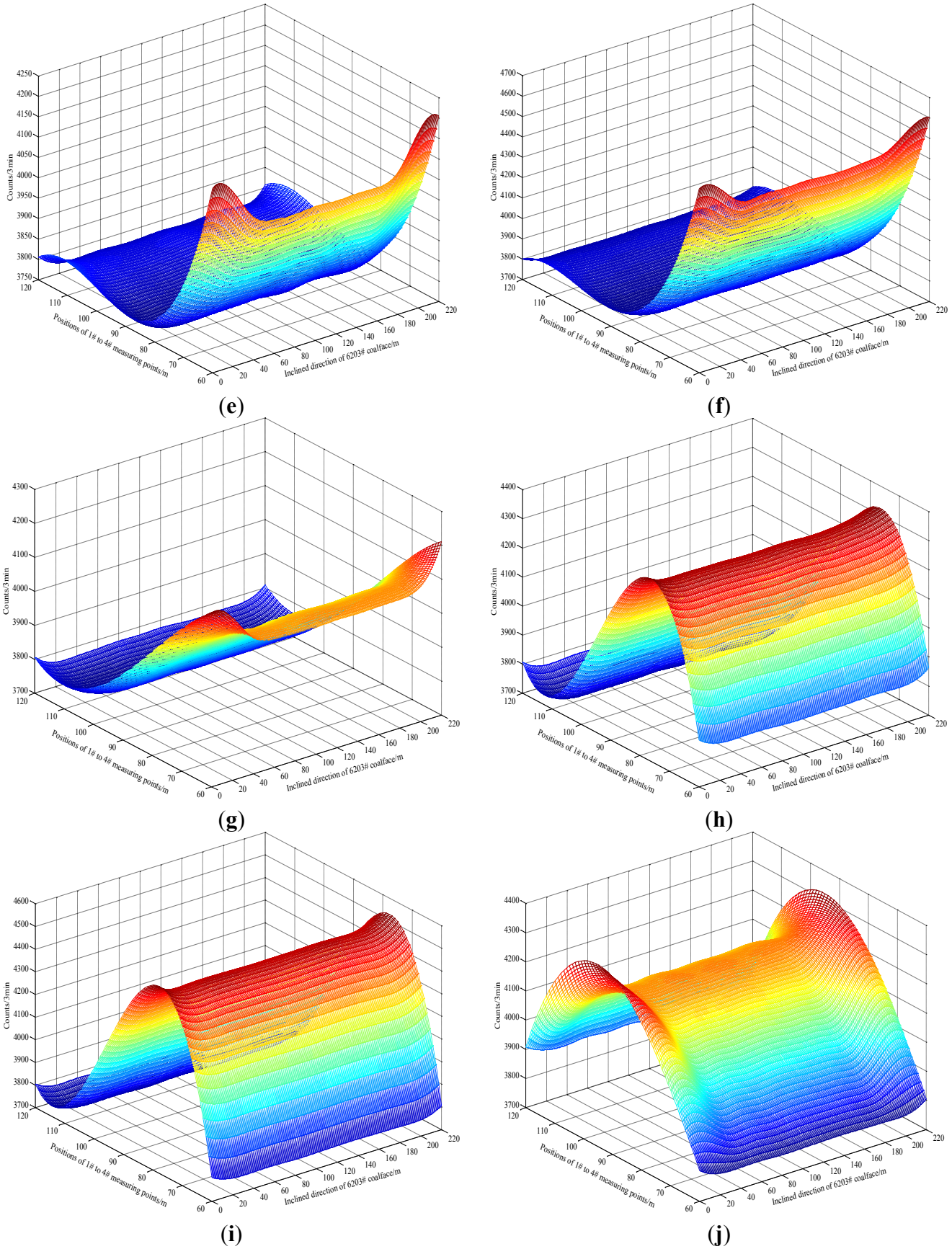

Figure 13. *Cont.*

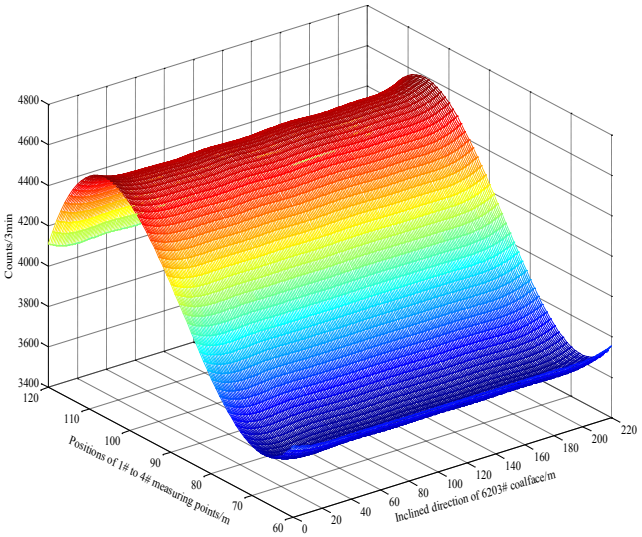

(k)

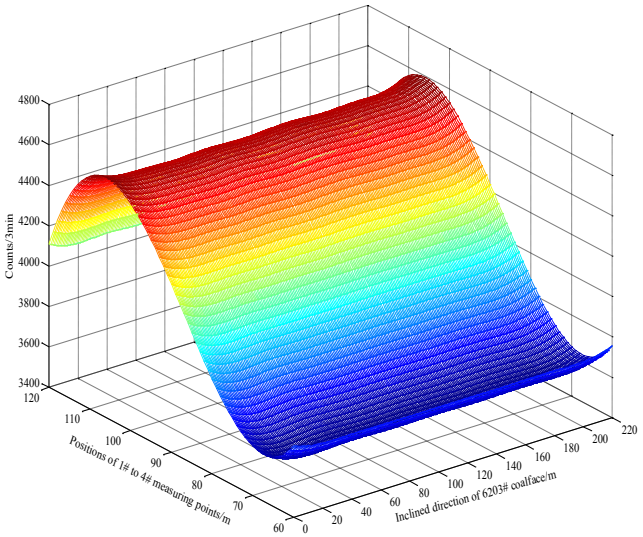

(l)

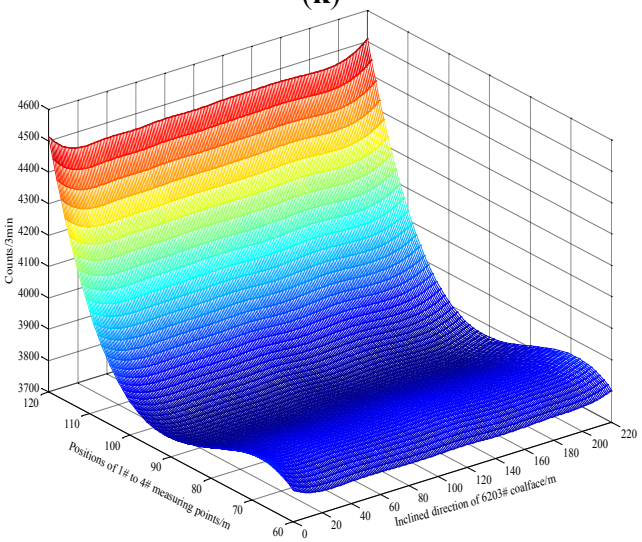

(m)

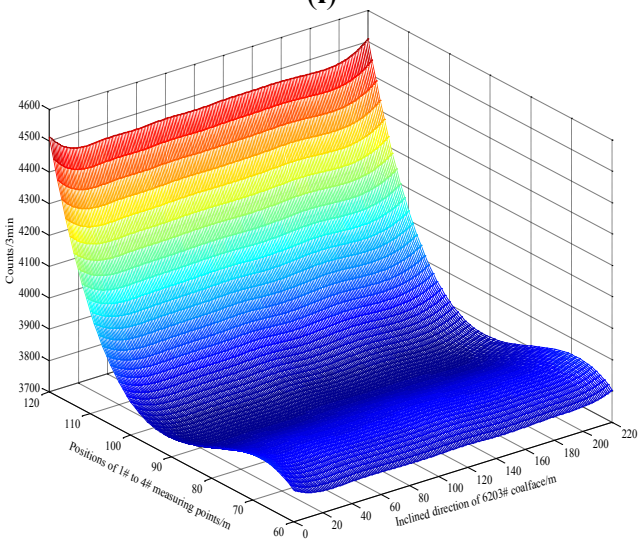

(n)

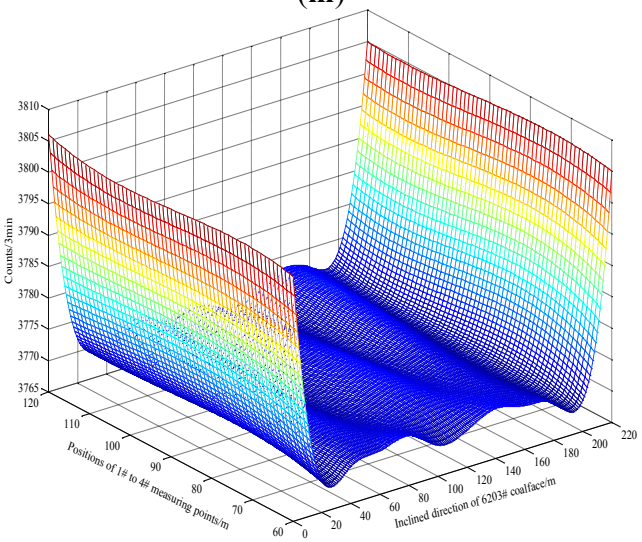

(o)

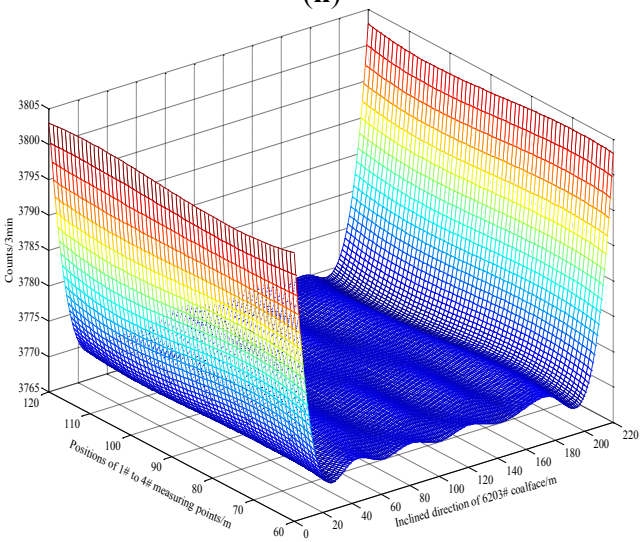

(p)

Figure 14. Variation features of the radon concentrations of ML 5: (**a**) 25 July to 28 July; (**b**) 29 July to 1 August; (**c**) 2 August to 5 August; and (**d**) 6 August to 9 August.

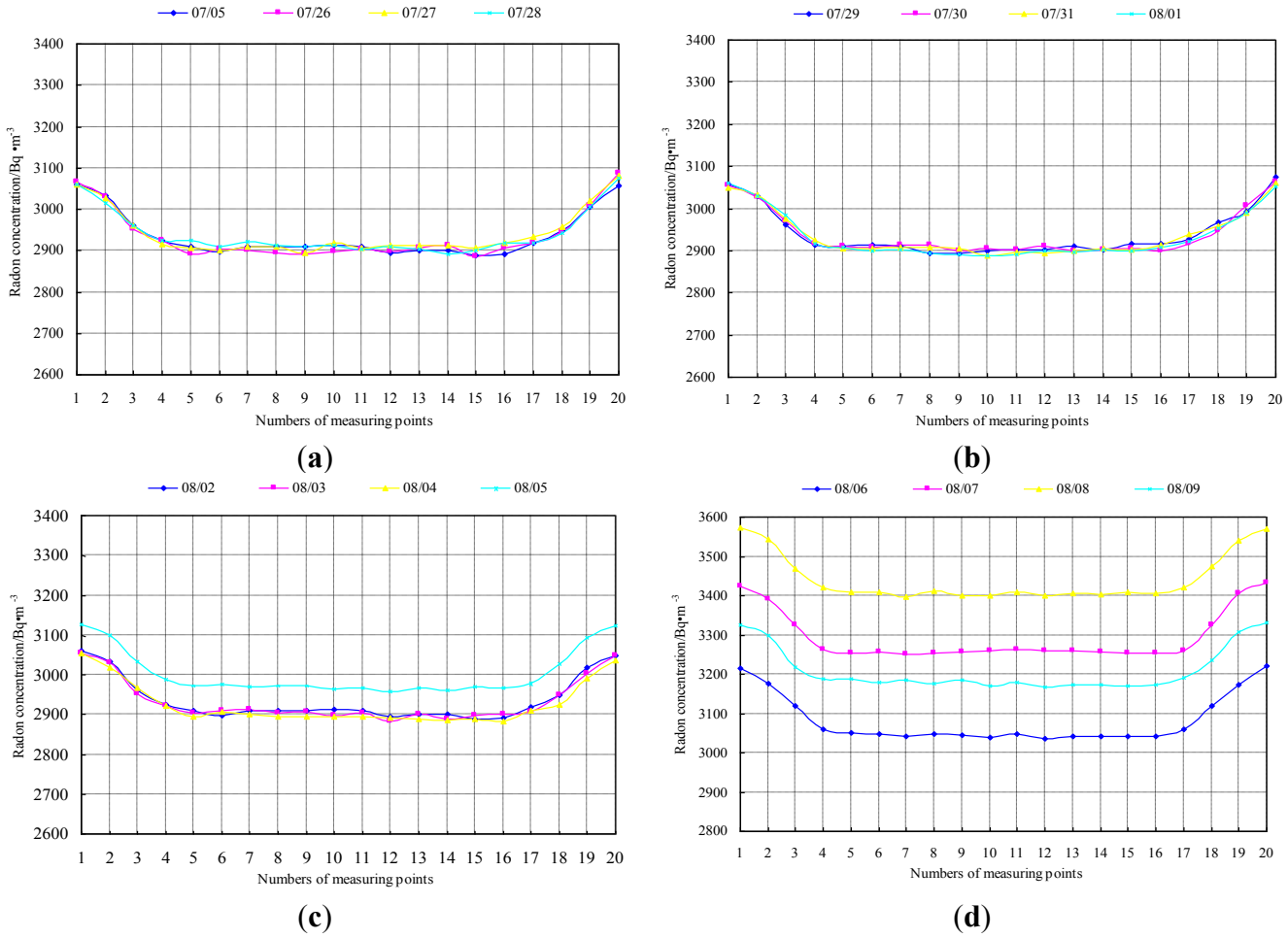

According to Figures 13 and 14, the average background concentration and counts near the two ends of the 6203# coalface were approximately 3060 and 3800 Bq/m^3, compared to approximately 2910 and 3770 Bq/m^3 in the middle of the 6203# coalface. The coal seam of the 6203# coalface was exploited from the open-off cut in 25 July 2011. When the coalface was advanced by 60 m, a considerable through crack appeared on the surface along the inclined direction of the coalface from 30 July to 31 July 2011, which is shown in Figure 15.

Figure 15. Through cracks on the surface during the first weighting.

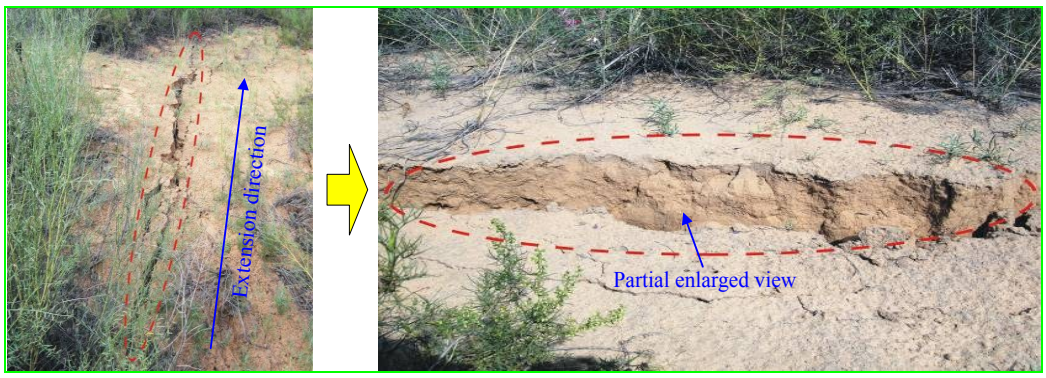

At this time, the maximum values were obtained on ML 1. The count values were approximately 4610 near the two ends and 4,480 in the middle area of the coalface, and the counts increased by 21.32% and 18.83% respectively relative to the average background counts. Thus, an inference can be made that the main roof in overlying strata generated the first breakage, and the coalface entered into a first weighting state. The weighting step was about 60 m, which coincided with the observation results of mine pressure from the KBJ-60III-1 continuous recorder for the working resistance of hydraulic supports in the 6203# coalface. Figure 16 gives an illustration of the working resistance of hydraulic supports in the 6203# coalface during the first weighting. When the coalface had advanced 20 m beyond ML 1, the longitudinal through cracks on the surface gradually closed, and the counts of each MP on ML 1 decreased from the maximum value to the background level.

Figure 16. The working resistance of hydraulic supports during the first weighting.

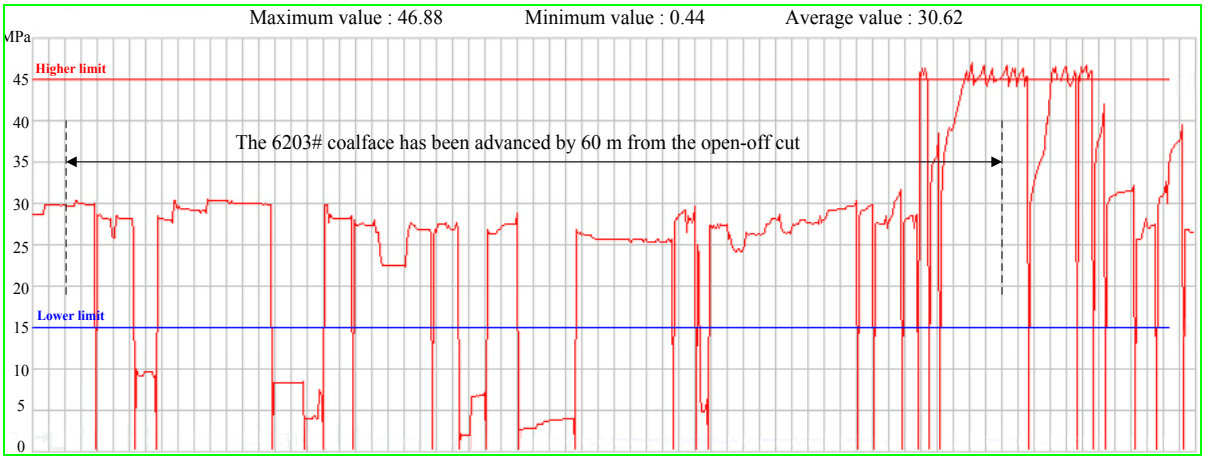

Figure 17. The relationships of through cracks, radon data and working resistance.

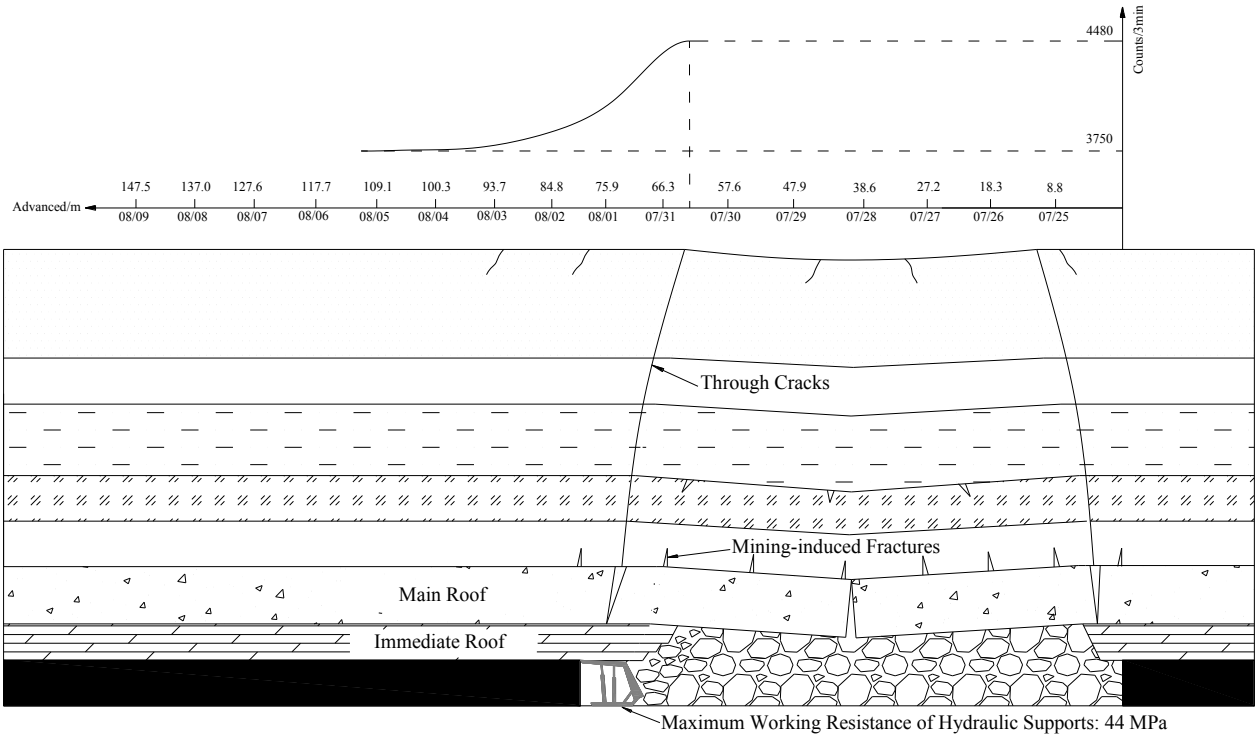

Figure 17 gives a depth section drawing to illustrate the relationships of through cracks, radon data and working resistance during the first weighting. Based on the measured data and the inference above, we can draw a conclusion that the main roof proceeded from the first periodic breakage, through the second, third and fourth periodic breakage as the coalface advanced. Simultaneously, the coalface progressed into the states of the first through the fourth periodic weighting with an average weighting step of 20 m, which is consistent with the observation results of underground mine pressure. The surface deformation and the working resistance of hydraulic supports are shown in Figures 18 and 19. During periodic weighting of the 6203# coalface, the maximum count values were approximately 4519 near the two ends and 4482 in the middle area of the coalface, an increase of approximately 18.92% and 18.89% from the average background counts.

Figure 18. Through cracks on the surface during the periodic weightings: (**a**) the first periodic weighting; (**b**) the second periodic weighting; (**c**) the third periodic weighting; and (**d**) the fourth periodic weighting.

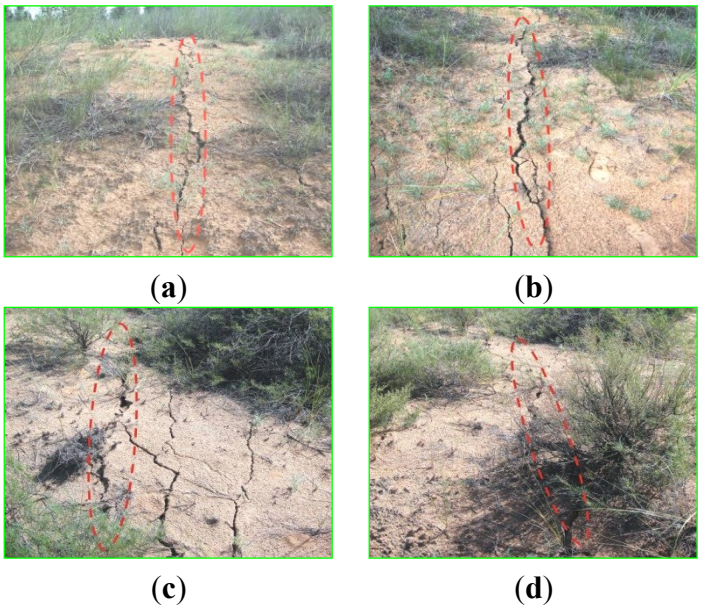

Figure 19. The working resistance of hydraulic supports during the periodic weightings.

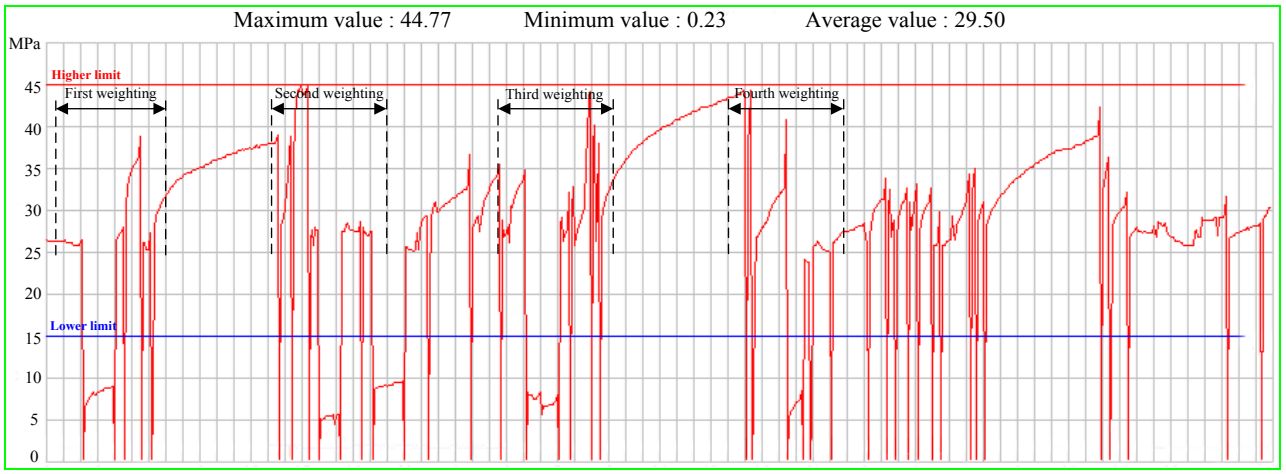

However, the maximum concentrations of radon were about 3573 and 3395 Bq/m^3, an increase of 16.76% and 16.67% from the average background concentrations. As the coalface advanced, the longitudinal through cracks on the surface gradually closed again. In addition, we can infer that the influence coverage of the advanced abutment pressure was equal to 30 m, which is consistent with the observation results of mining pressure

5. Discussion

In 1992, the Taiyuan University of Technology originally proposed the surface-based radon technique in China. This technique involves the measurement of the anomalous radon concentration in surface soil directly above a suspected subsurface coal heating and the relation of the anomaly to the heating process. Since then, this technique was applied to locate subsurface coal heating in several Chinese coal mines [27], resulting in some significant success. Since 2002, with the support of the Australian Coal Association Research Program (ACARP), the Commonwealth Scientific and Industrial Research Organization (CSIRO) has carried out detailed studies to apply and develop this technique in several Australian coal mines [28]. However, there is little published literature available on the radon detection of mining-induced fractures in the overlying strata on the surface during underground coal mining. The on-site detection results presented here indicate that the evolution of mining-induced fractures is significantly correlated with the variation of radon concentration. In order to understand how it occurs, some considerations must be made, including the source of radon, the mechanism of radon migration, the principle of radon detection technique, and the influence of uncertain factors.

5.1. The Source of Radon

Radon, Rn, is a zero group chemical element of the sixth cycle in the periodic table elements, and holds the atomic number 86. Three common radioactive radon isotopes occur in the natural environment: ^{219}Rn, ^{220}Rn and ^{222}Rn, the only one with a significantly long half-life is ^{222}Rn ($t_{1/2} \approx 3.82$ days) [29]. Generally speaking, radon refers to ^{222}Rn formed from the decay of ^{226}Ra in the natural ^{238}U decay series, as shown in Figure 20. Just as ^{238}U can be found in various types and amounts of coals, rocks, soils and waters on the earth's crust, radon is widespread in the natural environment. Rn, as a typical atmophile element, taking the form of gas in nature, is colorless and odorless, and is soluble in water and organic matter, and as well does not easily form a chemical reaction with other substances. However, its short-lived daughters are all solid and easily adsorbed by activated carbon, silica gel, polyethylene and some other materials. This property enables ^{222}Rn and its daughters to be easily collected from the surface of a container coated with these adsorbents and analyzed. The United Nations Scientific Committee on the Effects of Atomic Radiation (UNSCEAR) considers radon to be one of the most carcinogenic substances in the world [30]. Upon inhalation, radon can be lethal without any observable effect.

Figure 20. Decay process of the natural ^{238}U decay series.

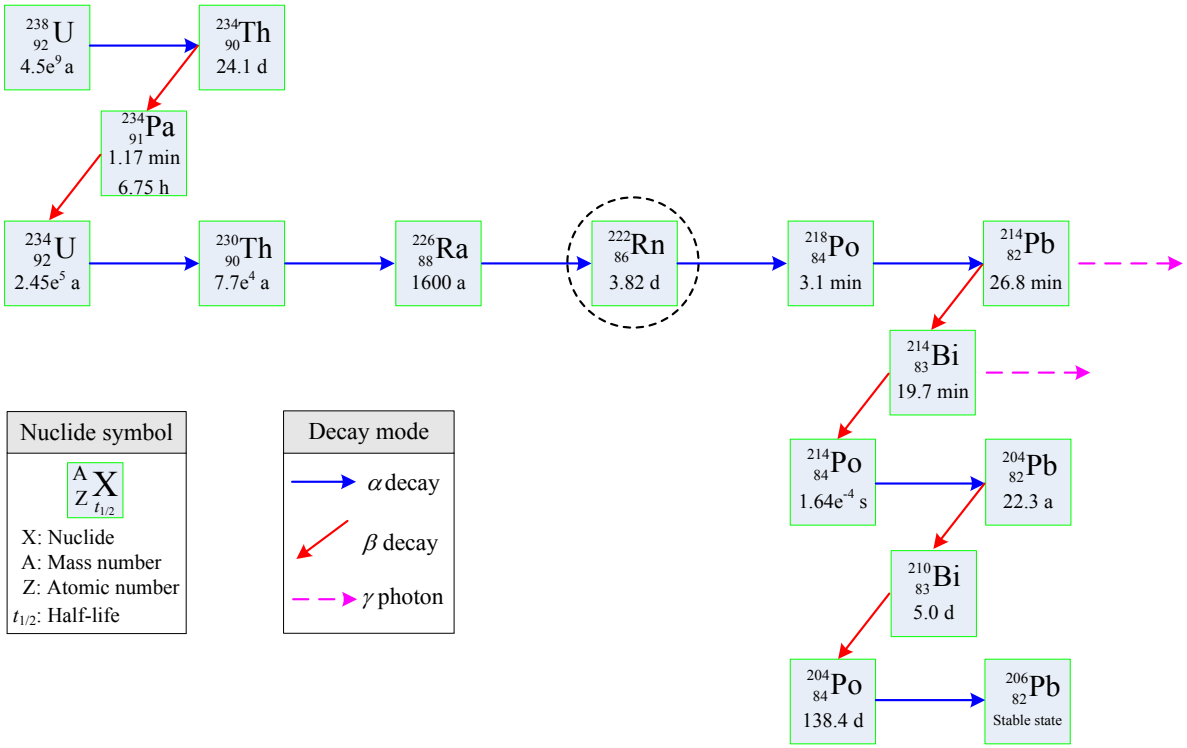

5.2. The Mechanism of Radon Migration

Radon has a strong migration ability under natural conditions. It can migrate in a gaseous or dissolved state within groundwater in geological environments. The migration of radon through the Earth is a well-documented phenomenon. For example, Kristiansson *et al.* [31] proved that a radon anomaly could be located at the surface above a strong radium source placed in a mine about 150 m beneath the surface with intermediate strata of quartzite and shale. Many studies have demonstrated that the Earth has been continuously exhaling gases (short-lived radon included) since then. Toutain *et al.* [32] used radon as a precursor, or an event indicator, for earthquakes and volcanic activity. The migration distance of radon from underground strata to the surface depends on different lithological characters, e.g., the vertical migration distance in homogeneous sand is 360 m to 420 m [33,34]. In addition, the increased phenomenon of radon concentration was observed in surface soil above coal spontaneous combustion areas at 400 m depths in China [35]. This phenomenon was also investigated on the surface vertically above the heating zones in Australian coal mines [36], suggesting that radon can migrate from underground strata at 400 m to 500 m depths to the surface.

Currently, most disputes focus on the mechanism that permits and drives radon migration. Radon was discovered in uranium products by the German scientist Dorn in 1900. Since then, many scholars have researched and proposed theoretical mechanisms of radon migration in the past 100 years. The mechanisms of radon migration can be roughly summed up as follows:

(a) Radon diffusion and convection. Fliigge and Zimens first proposed that radon migration was caused by the diffusion effect in 1939 [37,38]. They suggested that radon migrates from areas of high concentration to areas of low concentration, a migration based on the Fick Theorem. Fleisher and Mogro Campero were the first to propose that radon migration was driven by the

convection effect in 1979 [39,40]. Radon has been reported to travel considerable distances under the convection effect. However, many researchers have found that the combination of diffusion and convection is a viable migration mechanism for radon over distances of hundreds of meters [41,42].

(b) Pore-fluid drive. The underground fluid movement will cause dissolved radon to migrate with itself in the capillary interstice of subsurface strata, and the migration distance of radon depends on the flow velocity of underground fluid [43,44], a migration based on the Darcy Law.

(c) Microbubble hauling. Radon can be carried vertically as a stream of microbubbles, explaining both the rapid and vertical movement of radon [45]. These gas bubbles, mainly CO_2 and CH_4 could then carry other metallic elements and rare gases, such as Au, Cu, Pb, Zn, and Radon [46].

(d) Relay transmission. It may be radium to transmit radon and radon to transmit radon, also may be to rely on other matter or natural force. There are two types of transmission: two-step relay and multi-step relay. The authors think that the action of relay transmission may interpret the long migration of radon [47,48].

(e) Infinite source model. The build-up of stress prior to an earthquake or the release of the stress after the event can cause the change in strain field within the earth. This field is expected to extend to long distance if the earth acts as an elastic continuum. Wherever the ground is squeezed, the pore spaces are narrowed non-linearly and radon gas will be extruded. Wattananikorn *et al.* [49] considers that an earth model in which an infinite source is overlain by an overburden of thickness which contains no radon source.

(f) He-Rn cluster. Jia *et al.* [50] found that radon and most of its daughters and parents are decaying bodies that are able to radiate α-particles. After deceleration, the ^{4}He combine with ^{222}Rn and its daughters and parents to form He-Rn atomic clusters. When the buoyancy of air is greater than the gravity of the clusters, the self-ascending phenomenon occurs.

The upward migration process of radon is relatively intricate due to its particular properties, and the mechanism by which radon appears at the surface from underground strata is not fully understood. However, it is an indisputable fact that radon can migrate from underground to the surface along microfractures or micropores. The diffusion and convection effects are widely considered to be the primary mechanism of radon migration, which lays the theoretical basis for our research.

5.3. The Principle of Radon Detection Technique

^{222}Rn occurs naturally as a decay product of the long-lived ^{238}U, a common rare element in rock, coal, soil, and strata. Due to the influence of advanced mining-induced stress in the process of underground coal mining, mining-induced fractures in overlying strata develop and spread ahead of the coalface. In this case, radon can separate from rock, coal, soil, and strata, and then significantly migrate to the surface under the diffusion and convection effects in a unidirectional vertical direction. The migration speed and distance increase substantially with the development of mining-induced fractures. Due to the difference in fracture density, the numbers of escaping radon atoms will also be different. If the fracture develops well and forms the transfixion with the aquifer, the radon concentration will change significantly in the surface soil vertically above the fracture development zones. Based on the geological borehole data, we can know that which layers are aquifers and the

numbers of aquifers. On this basis, combining with the features of radon separation from different strata, the escaping radon from which layers can be distinguished. In addition, according to the radon anomalies in the surface soil, the information about the height and degree of mining-induced fractures development, and the communication with the aquifer, can be inversed. This is the basic principle of the radon technique for the detection of the development of mining-induced fractures in overlying strata.

5.4. Requirements for Future Research

The radon concentration in the strata is influenced by a number of factors. These may include the concentrations of uranium and thorium in the strata, the radon emanation power of the materials, the physical properties of the materials (e.g., the diffusion coefficient, the mineral particle size, the permeability, and the porosity) and environmental factors (e.g., the moisture content, the surrounding stress, and the temperature) [51–54]. However, the degree of influence of these factors varies with the different types of rock, coal, soil, and strata. The results reported in this paper are based on specific detection conditions and limited measured data. Nevertheless, the on-site detection results indicate that the mining-induced fractures in overlying strata can be qualitatively detected by using the radon technique on the surface. Therefore, in order to apply the radon technique to a wider spectrum for the detection of the mining-induced fractures in overlying strata with more certainty, additional studies are necessary such as the following:

(a) A series of laboratory tests are necessary in order to investigate the effect of uncertain factors, such as strata types, moisture content, and mineral particle size, on radon concentration in strata, especially reduce the degree of influence due to environmental factors that can affect the radon variability. This is the most elementary study for radon detection technique.

(b) How the mining-induced effect affects the movement of radon through strata? Although some numerical models of radon migration in soil have been proposed, there are few published studies available. Therefore, numerical modeling analysis is necessary to study the mining-induced effect on radon movement, in particular on its upright migration through underground multilayer strata. This study is of fundamental significance to the radon detection technique.

(c) More on-site detection work on mining-induced fractures in overlying strata by using radon technique on the surface should be undertaken. These studies should consider the effect of various mining and geological conditions for quantitative study on the development law of mining-induced fractures in overlying strata.

(d) If the conditions are allowable, the multi-parameter information should be synthetically considered. In recent years, some studies have investigated the detection of other forms of energy (e.g., acoustic emission, electromagnetic emission and neutron emission) as a reliable method for the monitoring of fracture phenomena and environmental protection against seismicity. For example, Carpinteri *et al.* [55] observed that energy emission during the failure process, clearly indicating charge redistribution, and neutron bursts, necessarily involving nuclear reactions, by subjecting quasi-brittle materials such as granite rocks to compression tests. Borla *et al.* [56] measured the electromagnetic pulses generated during micro-cracking of rock specimens by a dedicated loop antenna sensitive up to MHz, then took into account the relationship between electromagnetic emissions, neutron emissions and seismic activity, finally

considered that it would be possible to set up a sort of alarm system that could be at the base of a warning network. Therefore, we should consider using the detection of other forms of energy together with radon measurement for our research.

6. Conclusions

An on-site trial of radon detection of mining-induced fractures from overlying strata to the surface has been performed in the 6203# coalface of the BCM in China. The main conclusions of this paper can be summarized as follows:

(1) Due to its properties, the radon migration process is relatively intricate and the various mechanisms suggested for its transport through the overlying strata are not fully understood. However, the diffusion and convection effects are widely considered to be the primary mechanism of radon migration, which lays the theoretical basis for the relevant research.

(2) The on-site radon detection trial conducted in the 6203# coalface demonstrates that the first weighting step is about 60 m, and the average periodic weighting step is about 20 m. These values are consistent with the observation results of underground mine pressure. In addition, it is inferred that the influence coverage of the advanced abutment pressure is equal to 30 m.

(3) Although this study is based on specific detection conditions and limited measured data, the results suggest that the radon detection of mining-induced fractures from overlying strata to the surface is feasible. The radon detection technique may not directly help to prevent from any damage, as the damages (e.g., rock fracture, roof failure) already have happened during underground coal mining. Nevertheless, based on the detection results, the corresponding control measures of mining techniques (rapid advance, reducing mining height, localized backfill, grouting reinforcement, *etc*.) can be performed to reduce the development of the mining-induced fractures for the mitigation of safety issues as well as the adverse environmental consequences. Therefore, the new detection method should be generalized to account to the caused damage for the coal companies in western mining areas in China, which is also the long-term aim of this study.

(4) In order to apply the radon technique to the detection of mining-induced fractures in overlying strata with greater certainty, further studies are needed in future, such as a series of laboratory tests, numerical modeling analysis, more on-site detection work, and multi-parameter information consideration.

Acknowledgments

The research is financially supported by the National Basic Research Program of China (No. 2015CB251600), the National Natural Science Foundation of China (No. 51404254), the China Postdoctoral Science Foundation (No. 2014M560465), the Fundamental Research Funds for the Central Universities (No. 2013QNB24) and the Jiangsu Planned Projects for Postdoctoral Research Funds (No. 1302050B). We wish to thank the BCM for the support of on-site detection work, as well as Xiao-Fu Zhang from Inner Mongolia Yitai Coal Limited for the assistance of geological data collection. Special thanks are given to lecturer Jie-Qing Yu and assistant research fellow Juan-juan Li

from the China University of Mining & Technology for their language assistance. The authors are also grateful to the assistant editor Wen-Feng Zhu and three anonymous reviewers for their constructive comments and helpful recommendation.

Author Contributions

All the authors contributed to this paper. Wei Zhang performed the on-site detection work, prepared and edited the manuscript. Dong-Sheng Zhang provided theoretical and methodological guidance in the research process. Li-Xin Wu revised and reviewed the manuscript. Hong-Zhi Wang partially participated in literature search and data processing.

Conflicts of Interest

The authors declare no conflict of interest.

References

1. Yu, S.W.; Wei, Y.M. Prediction of China's coal production-environmental pollution based on a hybrid genetic algorithm-system dynamics model. *Energy Policy* **2012**, *42*, 521–529.
2. Chang, J.; Leung, D.Y.C.; Wu, C.Z.; Yuan, Z.H. A review on the energy production, consumption, and prospect of renewable energy in China. *Renew*. *Sust*. *Energy Rev.* **2003**, *7*, 453–468.
3. Zhou, H.D.; Wu, Q.; Fang, M.; Ren, Z.B.; Jin, L.F. Prediction of demand trends of coking coal in China based on grey linear regression composition model. *Int. J. Glob. Energy Issues* **2013**, *36*, 197–209.
4. Zhang, D.S.; Fan, G.W.; Liu, Y.D.; Ma, L.Q. Field trials of aquifer protection in longwall mining of shallow coal seams in China. *Int. J. Rock Mech. Min. Sci.* **2010**, *47*, 908–914.
5. Zhang, W.; Zhang, D.S.; Wu, L.X.; Wang, X.F. Numerical simulation on dynamic development features of mining induced fractures in overlying strata during shallow coal seam mining. *Electron*. *J. Geotech. Eng.* **2013**, *18*, 5531–5543.
6. Ma, L.Q.; Zhang, D.S.; Li, X.; Fan, G.W.; Zhao, Y.F. Technology of groundwater reservoir construction in goafs of shallow coalfields. *Int. J. Min. Sci. Technol.* **2009**, *19*, 730–735.
7. Yang, Y.K.; Kang, T.H.; Hao, X.L.; Zheng, T.B.; Wang, A. Research on in-situ purification technique of mine water in Shendong mining area. *Energy Educ. Sci. Tech.* **2012**, *29*, 209–216.
8. Li, G.Y.; Zhou, W.F. Impact of karst water on coal mining in North China. *Environ. Geol.* **2006**, *49*, 449–457.
9. Zhang, D.S.; Fan, G.W.; Ma, L.Q.; Wang, X.F. Aquifer protection during longwall mining of shallow coal seams: A case study in the Shendong Coalfield of China. *Int. J. Coal Geol* **2011**, *86*, 190–196.
10. Ma, L.Q.; Du, X.; Wang, F.; Liang, J.M. Water-preserved mining technology for shallow buried coal seam in ecologically-vulnerable coal field: A case study in the Shendong coal field of China. *Disaster Adv.* **2013**, *6*, 268–278.
11. Fan, G.W.; Zhang, D.S.; Zhai, D.Y.; Wang, X.F.; Lu, X. Laws and mechanisms of slope movement due to shallowly buried coal seam mining under ground gully. *J. Coal Sci. Eng.* **2009**, *15*, 346–350.

12. Zhang, J.C.; Peng, S.P. Water inrush and environmental impact of shallow seam mining. *Environ. Geol.* **2005**, *48*, 1068–1076.
13. Zhu, S.Y.; Jiang, Z.Q.; Cao, D.T.; Sun, Q.; Yang, C.W. Restriction function of lithology and its composite structure to deformation and failure of mining coal seam floor. *Nat. Hazards* **2013**, *68*, 483–495.
14. Wu, Q.; Wang, M.Y. Characterization of water bursting and discharge into underground mines with multilayered groundwater flow systems in the North China coal basin. *Hydrogeol. J.* **2006**, *14*, 882–893.
15. Lai, X.P.; Cai, M.F.; Xie, M.W. In situ monitoring and analysis of rock mass behavior prior to collapse of the main transport roadway in Linglong Gold Mine, China. *Int. J. Rock Mech. Min. Sci.* **2006**, *43*, 640–646.
16. Palchik, V. Localization of mining-induced horizontal fractures along rock layer interfaces in overburden: field measurements and prediction. *Environ. Geol.* **2005**, *48*, 68–80.
17. Zhang, S.T.; Liu, Y. A simple and efficient way to detect the mining induced water-conducting fractured zone in overlying strata. *Energy Proc.* **2012**, *16*, 70–75.
18. Qian, M.G.; Shi, P.W. *Mining Pressure and Strata Control*, 1st ed.; China University of Mining & Technology Press: Xuzhou, China, 2003. (In Chinese)
19. Lehmann, B.E.; Ihly, B.; Salzmann, S.; Conen, F.; Simon, E. An automatic static chamber for continuous ^{220}Rn and ^{222}Rn flux measurements from soil. *Radiat. Meas.* **2004**, *38*, 43–50.
20. Ciotoli, G.; Etiope, G.; Guerra, M.; Lombardi, S.; Duddridge, G.A.; Grainger, P. Migration of gas injected into a fault in low-permeability ground. *Q. J. Eng. Geol. Hydrogeol.* **2005**, *38*, 305–320.
21. Rohnsch, W.; Przyborowski, S.; Ettenhuber, E. Investigation and evaluation of the radiation exposure situation in uranium mining areas of Eastern Germany. *Radiat. Prot. Dosim.* **1992**, *45*, 127–132.
22. Zhang, W.; Zhang, D.S.; Wang, X.F.; Xu, M.T.; Wang, H.Z. Analysis of mathematical model for migration law of radon in underground multilayer strata. *Math. Probl. Eng.* **2014**, *2014*, 250852:1–250852:9.
23. Zhang, W.; Zhang, D.S.; Fan, G.W. Design of comprehensive test system for detecting overlying strata mining-induced fractures on surface with radon gas. *Int. J. Min. Sci. Technol.* **2011**, *21*, 823–827.
24. Zhang, W.; Zhang, D.S.; Ma, L.Q.; Wang, X.F.; Fan, G.W. Dynamic evolution characteristics of mining-induced fractures in overlying strata detected by radon. *Nucl. Sci. Tech.* **2011**, *22*, 334–337.
25. Winkler, R.; Ruckerbauer, F.; Bunzl, K. Radon concentration in soil gas: A comparison of the variability resulting from different methods, spatial heterogeneity and seasonal fluctuations. *Sci. Total Environ.* **2001**, *272*, 273–282.
26. Banjanac, R.; Udovicic, V.; Dragic, A.; Jokovic, D.; Maletic, D.; Veselinovic, N.; Grabez, B. Daily variations of gamma-ray background and radon concentration. *Rom. J. Phys.* **2013**, *58*, 14–21.
27. Wu, J.M.; Wu, X.W. Study and application of ^{222}Rn technique in coal mines. *China Coal* **1998**, *24*, 22–24. (In Chinese)
28. Xue, S.; Winkelmann, N. *Detection of Underground Spontaneous Combustion of Coal with Surface-Based Radon Technique at Dartbrook Mine*; University of Wollongong: Wollongong, Australia, 2005; pp. 265–270.

29. Luo, H.H.; Tang, D.Z.; Yan, Q.T.; He, W.; Xu, H. Radioactive elements in natural gas: A case study on distribution of gaseous ^{222}radon and its origin mechanism. *Nat. Hazards* **2012**, *63*, 647–657.
30. Lowe, S.; Pettenato, R. Reduction of indoor radon by air cleaning-case study. *J. Environ. Eng.* **2000**, *126*, 1125–1130.
31. Kristiansson, K.; Malmqvist, L. Evidence for nondiffusive transport of ^{222}Rn in the ground and a new physical model for the transport. *Geophys*. **1982**, *47*, 1444–1452.
32. Toutain, J.P.; Baubron, J.C. Gas geochemistry and seismotectonics: A review. *Tectonophysics* **1999**, *304*, 1–27.
33. Villalbaa, L.; Colmenero, S.L.; Montero, C.M.E.; Cano, J.A.; Renteria, V.M.; Delgado, M.C.J.; Jurado, T.L.A.; Davila, R.I.; Herrera, P.E.F. Radon concentrations in ground and drinking water in the state of Chihuahua, Mexico. *J. Environ. Radioact.* **2005**, *80*, 139–151.
34. Calugaru, D.G.; Crolet, J.M. Identification of radon transfer velocity coefficient between liquid and gaseous phases. *C.R. Mecanique* **2002**, *330*, 377–382.
35. Wu, J.M.; Gao, S.Q. Study on temperature detection technique at fire district of coal spontaneous combustion and its application. *China Saf. Sci. J.* **2004**, *14*, 109–112. (In Chinese)
36. Xue, S.; Dickson, B.; Wu, J. Application of ^{222}Rn technique to locate subsurface coal heatings in Australian coal mines. *Int. J. Coal Geol.* **2008**, *74*, 139–144.
37. Semkow, T.M.; Parekh, P.P. The role of Radium distribution and porosity in radon emanation from solids. *Geophys. Res. Lett.* **1990**, *17*, 456–465.
38. Shuleikin, V.N. Radon transport to the near-surface soil and air layers. *Izv. Atmos. Ocean. Phys.* **2013**, *49*, 853–859.
39. Gingrich, J.E. Radon as a geochemical exploration tool. *J. Geochem. Explor.* **1984**, *21*, 13–19.
40. Reimer, G.M. Reconnaissance techniques for determining soil-gas radon concentrations: An example from Prince Georges County, Maryland. *Geophys. Res. Lett.* **1990**, *17*, 809–812.
41. Pal, M.; Graaf, E.R.; Meijer, R.J.; Wit, M.H.; Hendriks, N.A. Experimental set-up for measuring diffusive and advective transport of radon through building materials. *Sci. Total Environ.* **2001**, *272*, 315–321.
42. Cheng, Y.X.; Wang, N.P.; Hou, S.L.; Liu, Q.C. Theoretical research on source of radon from earth into air. *Radiat. Prot. Bull.* **2001**, *21*, 15–18.
43. Wilkening, M.H.; Watkins, D.E. Air exchange and ^{222}Radon concentration in the Carlsbad Cavens. *Health Phys.* **1976**, *31*, 139–143.
44. Belikov, V.T.; Shestakov, A.F. Use of variations in radon concentration in determining spatial and temporal characteristics of destruction zones. *Russ. J. Nondestruct. Test.* **2000**, *36*, 231–236.
45. Varhegyi, A.; Hakl, J.; Monnin, M.; Morin, J.P.; Seidel, J.L. Experimental study of radon transport in water as test for a transportation microbubble model. *J. Appl. Geophys.* **1992**, *29*, 37–46.
46. Zhou, Z.Y.; Tao, S.; Xu, F.L.; Dawson, R. A physical-mathematical model for the transport of heavy metals and toxic matter from point sources by geogas microbubbles. *Ecol. Model.* **2003**, *161*, 139–149.
47. Wu, H.S.; Bai, Y.S.; Lin, Y.F.; Chang, G.L. The action of relay transmission of the radon migration. *Chin. J. Geophys.* **1997**, *40*, 136–142. (In Chinese)
48. Folger, P.F.; Poeter, E.; Wantye, R.B.; Day, W.; Frishman, D. ^{222}Rn transport in fractured crystalline rock aquifer: results from numerical simulations. *J. Hydrol.* **1997**, *195*, 45–57.

49. Wattananikorn, K.; Kanaree, M.; Wiboolsake, S. Soil gas radon as an earthquake precursor: Some considerations on data improvement. *Radiat. Meas.* **1998**, *29*, 593–598.
50. Jia, W.Y.; Fang, F.; Zhou, R.S.; Ma, Y.J.; Qiu, Y.D.; Hou, X.S.; Wu, Y.P.; Zu, X.L.; Wang, X.Q. Internal causes of radon and its daughters upward migration and cluster phenomenon. *J. Chengdu Univ. Technol.* **1999**, *26*, 171–175. (In Chinese)
51. Nazaroff, W.W. Radon transport from soil to air. *Rev. Geophys.* **1992**, *30*, 137–160.
52. Sun, H.B.; Furbish, D.J. Moisture content effect on radon emanation in porous media. *J. Contam. Hydrol.* **1995**, *18*, 239–255.
53. Hutter, A.R. Spatial and temporal variations of soil gas ^{220}Rn and ^{222}Rn at two sites in New Jersey. *Environ. Int.* **1996**, *22*, 455–469.
54. Xue, S.; Wang, J.; Xie, J.; Wu, J. A laboratory study on the temperature dependence of the radon concentration in coal. *Int. J. Coal Geol.* **2010**, *83*, 82–84.
55. Carpinteri, A.; Lacidogna, G.; Borla, O.; Manuello, A.; Niccolini, G. Electromagnetic and neutron emissions from brittle rocks failure: Experimental evidence and geological implications. *Sadhana* **2012**, *37*, 59–78.
56. Borla, O.; Lacidogna, G.; Battista, E.D.; Niccolini, G.; Carpinteri, A. Electromagnetic emission as failure precursor phenomenon for seismic activity monitoring. *Fract. Fatigue Fail. Damage Evol.* **2015**, *5*, 221–229.